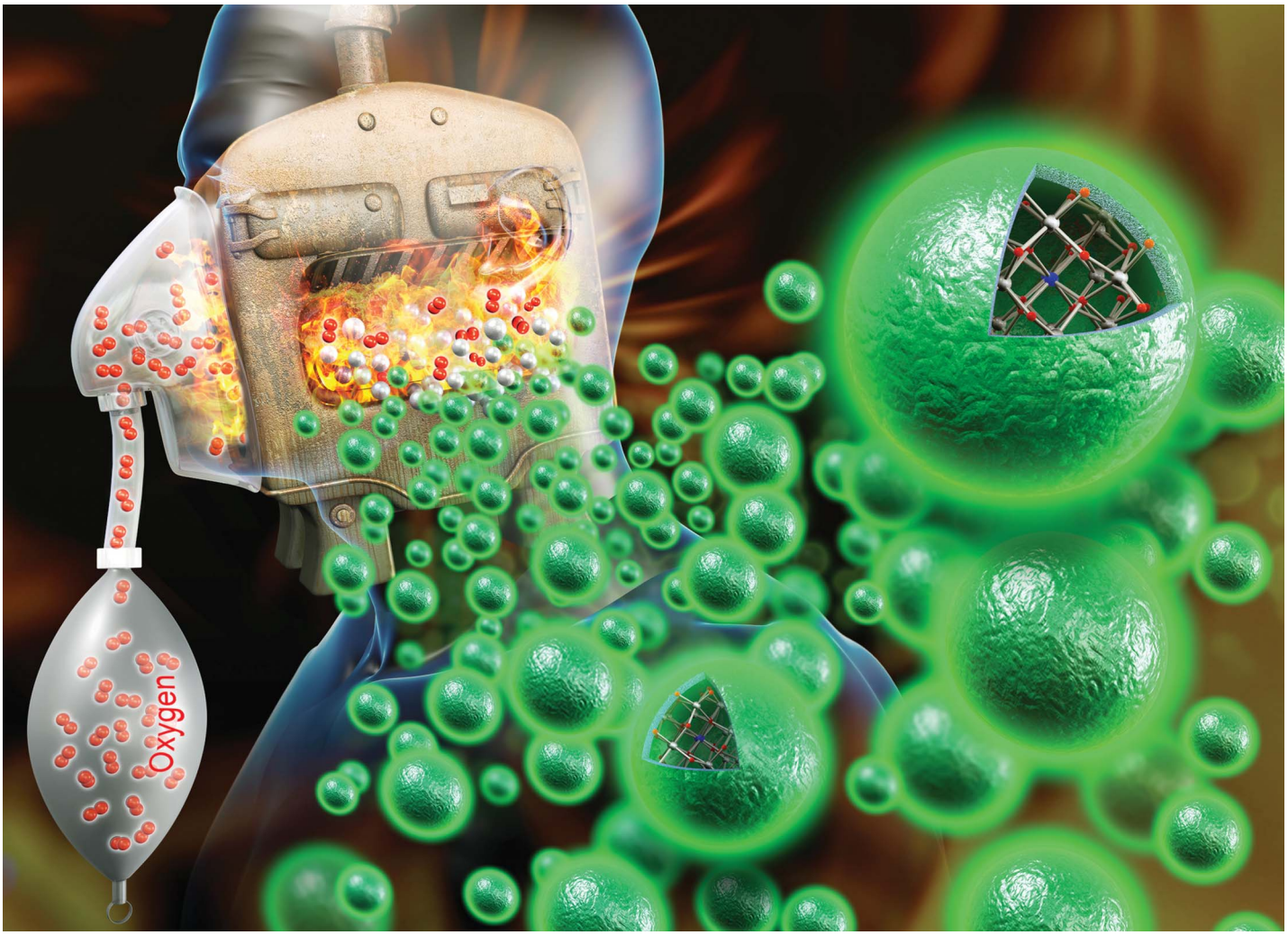

Simulation-guided phosphor fabrication research from S. Kim and S. H. Cho's teams at Korea Institute of Science and Technology.

Title: Roles of an oxygen Frenkel pair in the photoluminescence of Bi^{3+}-doped Y_2O_3: computational predictions and experimental verifications

Improved photoluminescence efficiency of Bi-doped Yttria by supplying oxygen gas during the sample annealing.

As featured in:

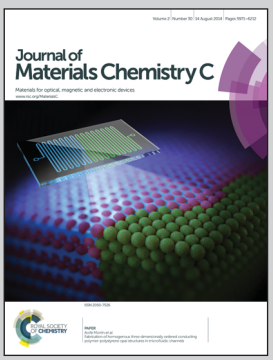

See Seungchul Kim *et al.*, *J. Mater. Chem. C*, 2014, **2**, 6017.

ROYAL SOCIETY OF CHEMISTRY

www.rsc.org/MaterialsC

Registered charity number: 207890

Journal of Materials Chemistry C

PAPER

View Article Online
View Journal | View Issue

Cite this: J. Mater. Chem. C, 2014, 2, 6017

Roles of an oxygen Frenkel pair in the photoluminescence of Bi^{3+}-doped Y_2O_3: computational predictions and experimental verifications

Heechae Choi,[a] So Hye Cho,[bc] Sovann Khan,[bc] Kwang-Ryeol Lee[a] and Seungchul Kim*[a]

Received 5th March 2014
Accepted 23rd May 2014

DOI: 10.1039/c4tc00438h

www.rsc.org/MaterialsC

Bi^{3+} as a dopant in wide-band-gap yttria (Y_2O_3) has been used as a green light emission center or a sensitizer of co-doped rare earth elements. Because the photoluminescence (PL) properties of Y_2O_3:Bi^{3+} vary remarkably according to heat treatment, the roles of point defects have been an open question. By using first-principles calculations and thermodynamic modeling, we have thoroughly investigated the formation of point defects in Y_2O_3:Bi^{3+} at varying oxygen partial pressures and temperatures, as well as their roles in PL. The photoabsorption energies of the Bi^{3+} dopant were predicted to be 3.1 eV and 3.4 eV for doping at the S_6 and the C_2 sites, respectively, values that are in good agreement with the experimental values. It was predicted that an oxygen interstitial (O_i) and an oxygen vacancy (V_O) are the dominant defects of Y_2O_3:Bi^{3+} at ambient pressure and an annealing temperature of 1300 K (3.19×10^{16} cm^{-3} for 1% Bi doping), and the concentrations of these defects in doped Y_2O_3 are approximately two orders of magnitude higher than those in undoped Y_2O_3. The defect V_O^{2+} in Y_2O_3:Bi^{3+} was predicted to reduce the intensity of PL from Bi^{3+} at both S_6 and C_2 sites. We verify our computational predictions from our experiments that the stronger PL of both 410 and 500 nm wavelengths was measured for the samples annealed at higher oxygen partial pressure.

Introduction

Transparent bixbyite yttria (Y_2O_3) has been widely used as a host material for trivalent rare earth (RE) dopants, or *activators*, which emit photons in the visible light or the near-infrared (NIR) ranges.[1–5] Its wide band gap (5.5 eV) and low phonon vibrations make yttria a suitable host material for a wide emission range of phosphors. For instance, Eu^{3+}-co-doped yttria is used as the best quality material for producing a red light emitting diode (LED), and Yb^{3+}-co-doped yttria emits at NIR wavelengths.[5,6]

Bi^{3+}-doped Y_2O_3 (Y_2O_3:Bi^{3+}) has been suggested as a green light (500 nm) emission source, or a sensitizer, to increase the PL intensity from co-doped RE activators.[6–12] The green light emission or sensitization of Bi^{3+} occurs when photons are absorbed by Bi^{3+} at Y-sites, by the $6s^2 \rightarrow 6s6p$ transition, followed by sequential emission or energy transfer to the activators by the $6s6p \rightarrow 6s^2$ transition of Bi^{3+}.[6–10] Bi^{3+} absorbs two ranges of wavelengths, 325–346 nm and 370–378 nm, at two nonequivalent sites of yttrium, S_6 and C_2.[7–10] The S_6 and the C_2 sites are known to emit photons, at 410 and 500 nm, respectively.

The RE activators in Bi^{3+}-doped yttria efficiently absorb photons mostly at 500 nm, which are emitted from the Bi^{3+} at the C_2 site.[7–10] For a higher efficiency of energy conversion in a Bi^{3+}-sensitized phosphor, the host lattice should have high crystallinity so that the emission peak from Bi^{3+} at the C_2 site becomes sharp and intense. In addition, the sensitizer–activator distance should be closer because the energy transfer efficiency η_{eff} follows the relation, $\eta_{eff} \propto 1/R_{SA}^6$, where R_{SA} is the sensitizer–activator distance. Therefore, the PL intensity increases with the doping concentration of the RE activator up to a certain limit.

Recently, combustion techniques and colloidal methods have been used to synthesize yttria nanophosphors.[11–13] These methods are followed by high-temperature annealing (~1300 K) for increasing the crystallinity and removing the radicals. For Y_2O_3:Bi^{3+} synthesis, the former method is more frequently employed. The optimized Bi mole percentage that gives the best PL intensity and peak broadness by Bi^{3+} at the S_6 and the C_2 sites is heavily influenced by several fabrication conditions.[10–14]

[a]Center for Computational Science, Korea Institute of Science and Technology, Hwarangro 14 Gil 5, 136-791, Seoul, Korea. E-mail: sckim@kist.re.kr; Fax: +82 2 958 5451; Tel: +82 2 958 5491

[b]Center for Materials Archtecturing, Korea Institute of Science and Technology, Hwarangro 14 Gil 5, 136-791, Seoul, Korea

[c]Department of Nanomaterial Science and Engineering, Korea University of Science and Technology, 217 Gajeong-ro Yuseong-gu, Daejeon, 305-350, Korea

For example, Jacobsohn *et al.* reported that the type of combustion fuel affects the PL properties; in particular, they showed that urea as the fuel gives the best peak sharpness with equal intensities from Bi^{3+} at the S_6 and the C_2 sites[14]. The work of Huang,[10] which used a longer annealing time, however, showed a weaker and a broader PL peak from Bi^{3+} at the C_2 site than that from the S_6 site, despite the use of identical chemical starting materials and fuels as for the study of Jacobsohn.

The origin of this discrepancy in the optical properties mostly falls into two categories: the formation of a variety of phases or the introduction of native defects. It is reasonable to exclude the formation of a variety of phases for Y_2O_3:Bi^{3+} synthesis because X-ray diffraction (XRD) measurements demonstrated the uniform bixbyite structure after an annealing process.[7–11,14] Therefore, native defects and defect doping with H, C or N atoms can exist and influence the optical properties of the crystals, as can be seen in other phosphor materials that have been well-studied theoretically, such as GaN and ZnO.[15–19] However, the conditions of the heat treatment also significantly alter the peak broadness and intensity; hence, the roles of the native defects are important in the Y_2O_3:Bi^{3+} system.

We theoretically investigated the formation of native point defects in Y_2O_3:Bi^{3+} under the experimentally employed conditions for the annealing temperature and the oxygen pressure, as well as their roles in the PL properties. Based on the defect energy levels, we predicted the absorption wavelengths of each defect system. Our defect modeling includes dopant–defect complexes to thoroughly investigate the effects of doped Bi on the energetic stability and the energy levels of point defects. In addition, we prepared Y_2O_3:Bi^{3+} phosphors under oxygen-poor, ambient, and oxygen-rich conditions and compared their PL intensities. The result showed good agreement between the theoretical predictions and experimental outputs.

Calculation methods

We performed density functional theory (DFT) calculations within the generalized gradient approximation (GGA), with Perdew–Burke–Ernzerhof (PBE) parameterization.[25,26] We used VASP software,[21] and atomic nuclei and core electrons were described by a projector-augmented wave (PAW) method.[24] Khon–Sham orbitals[20] were expanded with a cutoff energy of 450 eV, and a $3 \times 3 \times 3$ equally spaced *k*-point grid was used for Brillouin zone sampling. A Hubbard *U* approximation ($U_{5d} = 6$ eV) term[27] was included to correct the splitting of the 5*d* orbital of yttrium, and the spin–orbit coupling (SOC) was included for the correct description of the bismuth orbitals. With the SOC term, our calculations agreed well with the experimental observations of the 6*s* and the 6*p* states of bismuth.[6–12] In the formation energy calculations, the experimental binding energy of an oxygen molecule, 2.56 eV per atom, was employed instead of the GGA value, which is known to significantly overestimate the bonding energy of the O_2 molecule.[28] The yttria unit cell contains 32 yttrium atoms (8 at the S_6 sites and 24 at the C_2 sites) and 48 oxygen atoms, as presented in Fig. 1. The cell volume and all atoms were fully relaxed. The Bi^{3+}-doped Y_2O_3 was modeled with the incorporation of one Bi^{3+} ion at an interstitial site (Bi_i) or at two yttrium sites, S_6 and C_2.

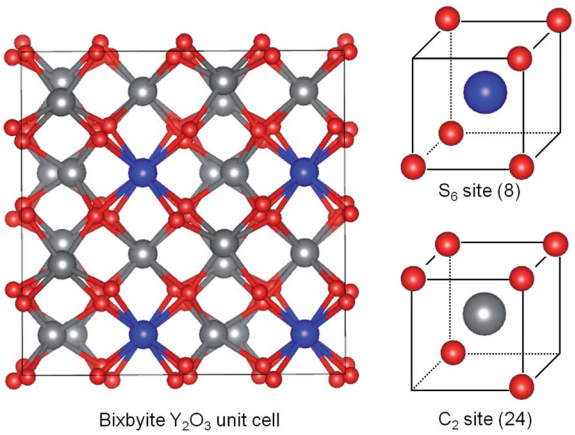

Fig. 1 Atomic model of the bixbyite structure. Red spheres are O atoms, and blue and grey spheres are Y atoms at the S_6 and the C_2 sites, respectively. The numbers in the parentheses are the number of the S_6 and the C_2 sites in the primitive unit cell.

Results and discussion

a. Formation energies and electronic structures of Y_2O_3 and Y_2O_3:Bi

The formation energy of yttria ($\Delta E^{f}_{Y_2O_3}$) was calculated using the equation

$$\Delta E^{f}_{Y_2O_3} = E_{Y_2O_3} - 2E_Y - \frac{3}{2}E_{O_2}, \quad (1)$$

where $E_{Y_2O_3}$, E_Y and E_{O_2} are the total energies of the yttria crystal, solid yttrium, and an isolated oxygen molecule, respectively. The formation energy ($\Delta E^{f}_{Y_2O_3}$), the lattice constant and the band gap of yttria are presented in Table 1, along with a comparison to the values from a previous DFT study[23] performed using the GGA functional of Perdew–Wang (PW91)[21] and an experimental study.[29] The formation energy and the lattice constant from the PBE calculations are very close to the experimental values, as is shown in Table 1. The band gap was underestimated in the PBE calculations, whereas it was corrected to nearly the experimental value by inclusion of *U* ($U_{5d} = 6$ eV). The SOC term gives rise to negligible changes in the band gap of yttria.

The free energy of Bi-doping was calculated using the chemical reactions below (reactions I, II and III). Temperatures

Table 1 Calculated and experimental formation energies (ΔE^{f}) per formula unit, lattice constant, and band gap of Y_2O_3

	ΔE^{f} (eV per f.u.)	Lattice constant (Å)	Band gap (eV)
PW (ref. 21)	−19.41	10.700	4.1
PBE (this work)	−20.47	10.605	4.6
PBE + *U* (this work)	—	—	5.3
Experiment (ref. 22)	−20.29	10.604	5.5

of 800 and 1300 K were considered because combustion and annealing were performed at these temperatures in many reported experiments.[7–10] The solid and liquid phases of bismuth oxide (Bi_2O_3) were considered as references for the bismuth chemical potential for 800 and 1300 K, respectively, because the melting point is 1100 K.[11,14]

Substitution of Y:

$$\left(1-\frac{1}{2}x\right)Y_2O_3+\frac{x}{2}Bi_2O_3+\Delta G^{f}_{Y_2O_3}\leftrightarrow Y_{2-x}Bi_xO_3. \quad (I)$$

Substitution of O (anti-site):

$$Y_2O_3+\frac{x}{2}Bi_2O_3+\Delta G^{f}_{Y_2O_3:Bi}\leftrightarrow Y_2Bi_xO_{3-x}+\frac{5x}{4}O_{2(g)}. \quad (II)$$

Bi interstitial:

$$Y_2O_3+\frac{x}{2}Bi_2O_3+\Delta G^{f}_{Y_2O_3:Bi}\leftrightarrow Y_2Bi_xO_3+\frac{3x}{4}O_{2(g)}. \quad (III)$$

The Bi-doping energy ($\Delta G^{f}_{Y_2O_3:Bi}$) is the change in the free energy by Bi-doping per Bi atom. In our calculations of $\Delta G^{f}_{Y_2O_3:Bi}$, the thermal energies of the solids (Y_2O_3:Bi, Y_2O_3 and Bi_2O_3) were ignored because their contributions to $\Delta G^{f}_{Y_2O_3:Bi}$ would be largely cancelled out. Hence, the Gibbs free energies can be replaced by the calculated total energies of Y_2O_3:Bi and Y_2O_3. The calculated $\Delta G^{f}_{Y_2O_3:Bi}$ under extremely oxidizing and reducing conditions at 298 K are listed in Table 2. The upper limit of the oxygen chemical potential, which is under extremely oxidizing conditions, is given by

$$\mu_O \leq \mu^0_O = \frac{1}{2}E_{O_2}. \quad (2)$$

The lower limit can be defined when yttria is decomposed into solid yttrium and oxygen gas. Thus, $\mu_Y = \mu^0_Y = E_Y$ under extremely reducing conditions, where E_Y is the total energy of yttrium in the solid phase. The chemical potential of oxygen was calculated using the thermodynamic equation for ideal gases and the chemical potential at standard temperature and pressure. As the reference point, μ^0_O is used as the zero point:

$$\Delta\mu_O = \mu_O - \mu^0_O. \quad (3)$$

The oxygen chemical potential was expressed as

$$\Delta\mu_O(T, P_{O_2}) = \frac{1}{2}\left\{\tilde{\mu}_{O_2}(T, P^0) + k_B T \ln\left(\frac{P_{O_2}}{P^0}\right)\right\}, \quad (4)$$

where $\tilde{\mu}_{O_2}(T, P^0)$ is the O_2 chemical potential at standard pressure (P^0) and temperature T.[30]

The Bi-doping energies ($\Delta G^{f}_{Y_2O_3:Bi}$) of the reactions considered are listed in Table 2 and are plotted in Fig. 2 for the two representative temperatures of 800 K and 1300 K with varying oxygen pressures. The experimental heat of fusion of Bi_2O_3, 6.8 kcal mol^{-1} (0.30 eV per f.u.),[31] was added to the formation energy for calculations at 1300 K, which is higher than the melting temperature of Bi_2O_3. Our calculations show that substitutional Bi^{3+} doping at the S_6 site is more favorable than at the C_2 site by the energy difference of 0.08 eV. The preference of Bi^{3+} at S_6 is consistent with the tendency found in the Stanek's simulation work using Buckingham potentials: a dopant with a larger ionic radius than the host cation favors the S_6 site of an oxide in the bixbyite structure.[32] Bi as an interstitial or an anti-site defect is very high in energy under atmospheric conditions. Obeying the Boltzmann factor, $N_{Bi_{C_2}}/N_{Bi_{S_6}} = \frac{N_{C_2}}{N_{S_6}}\exp\left[\frac{E_{Bi_{S_6}} - E_{Bi_{C_2}}}{k_B T}\right]$, the Bi^{3+} populations at the S_6 and the C_2 sites are in the ratio of 1 : 0.94 at 800 K, and 1 : 1.47 at 1300 K. At higher temperature, the pre-exponential factor $\left(\frac{N_{C_2}}{N_{S_6}} = 3\right)$ becomes more important than the energy difference, such that the population at the C_2 sites becomes larger. The tendency for an increase in the amount of Bi^{3+} at the C_2 sites as the temperature increases is consistent with the tendency for an increase in the amount of Bi at the C_2 sites when a fuel with a large heat of combustion was used.[14]

The localized 6*s*- and 6*p*-orbitals of Bi^{3+} appear very clearly in the electron density of states (DOS) in Fig. 3. The separation of the 6*s*- and the 6*p*-orbitals was not described well without the SOC. The Bi^{3+} at both the S_6 and the C_2 sites has sharply localized 6*s*- (occupied) and 6*p*- (unoccupied) orbitals within the band gap of the yttria host. The calculated energy distances

Table 2 Bi doping energies at 298 K and the corresponding lattice constants

Doping type	Net charge (*e*)	Bi-doping energy (eV per Bi-atom) $\mu_O = \mu^0_O$	Bi-doping energy (eV per Bi-atom) $\mu_Y = \mu^0_Y$	Lattice constant (Å)
Bi_{S_6}	0	−0.60	−0.60	10.613
Bi_{C_2}	0	−0.52	−0.52	10.612
Bi_O	0	14.04	3.04	10.668
	+1	9.78	−1.22	10.648
	+2	6.29	−4.71	10.629
	+3	2.38	−8.62	10.595
Bi_i	0	13.44	6.84	10.678
	+1	11.36	4.76	10.650
	+2	10.54	3.94	10.629
	+3	9.62	3.02	10.610

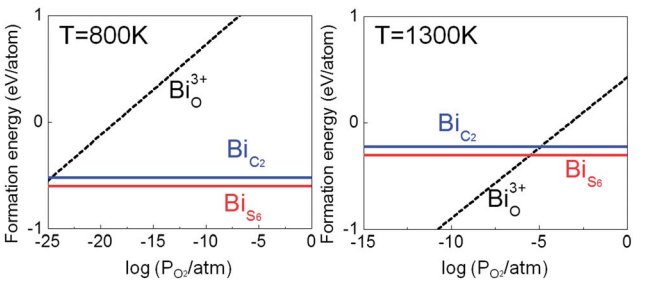

Fig. 2 The calculated Bi doping energy ($\Delta G^{f}_{Y_2O_3:Bi}$) as a function of P_{O_2} at 800 K and 1300 K. Anti-site (Bi_O) doping becomes dominant below $P_{O_2} = 4.0 \times 10^{-26}$ atm at 800 K and $P_{O_2} = 2.5 \times 10^{-6}$ atm at 1300 K.

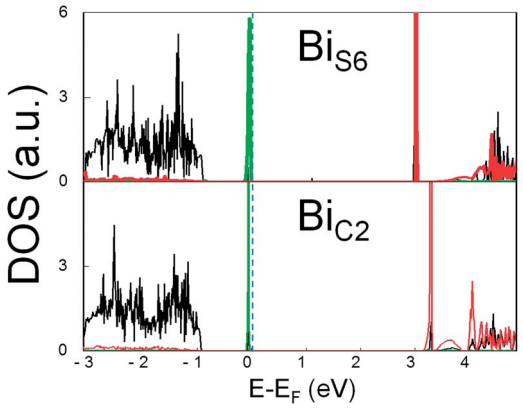

Fig. 3 Electron density of states of Bi-doped Y_2O_3. Green and red curves are PDOS of Bi6*s* and 6*p*, and the black curve is the total DOS. The black curves were normalized by the number of atoms.

between the in-gap 6*s*- and 6*p*-orbitals are 3.10 (400 nm) and 3.42 eV (362 nm) for the S_6 and the C_2 sites, respectively. The wavelengths of excitation correspond to the 6*s*–6*p* separations, which lead to the $^1S_0 \rightarrow {}^1P_1$ transitions being slightly longer than the experimental measurements, 378 nm and 325 nm.[7,8,10,14] One common method to correct the energy levels for an underestimated band gap is to rigidly shift the occupied states and the unoccupied states as much as the gap under estimation, while fixing the level intervals between the occupied states and between the unoccupied states. With this method, the corrected $^1S_0 \rightarrow {}^1P_1$ transition wavelengths of Bi^{3+} at the S_6 and the C_2 sites are 376 and 342 nm, respectively, which agrees very well with the experiments.

Because the photoexcitation by Bi^{3+} occurs between the states within the band gap of the host material, the sensitized luminescence of Y_2O_3:Bi^{3+}-RE does not follow the theoretical scheme of Mott and Gurney,[33] in which the electrons and holes recombine at the activator ions. The energy transfer with a 500 nm photon emitted from Bi^{3+} at the C_2 site mainly contributes to the sensitization.

b. Defect formation in Y_2O_3 and Y_2O_3:Bi

We calculated the point defect formation energies of Y_2O_3 and Y_2O_3:Bi^{3+} within the chemical potential ranges of Y and O, given by

$$\mu_Y^0 + \frac{1}{2}\Delta E^f_{Y_2O_3} < \mu_Y \leq \mu_Y^0 \quad (5)$$

and

$$\mu_O^0 + \frac{1}{3}\Delta E^f_{Y_2O_3} < \mu_O \leq \mu_O^0. \quad (6)$$

We considered the native point defects of pure Y_2O_3 to be oxygen vacancies (V_O), yttrium vacancies at the S_6 (V_{S_6}) and the C_2 (V_{C_2}) sites and interstitial oxygen (O_i) and yttrium (Y_i). In addition, we also included the complexes of each point defect and bismuth at the nearest distance to investigate the affinity of point defects for the bismuth dopant, which may change the defect concentrations and electronic structures. We also considered the defect to be charged.

Eqn (7) gives the defect formation energies of point defects with a charge q ($\Delta E^f(q)$), as a function of the Fermi level, using the equation:

$$\Delta E^f(q) = E[D^q] \pm \mu_i - E^0 + q(E_v + \Delta V + \varepsilon_F), \quad (7)$$

where $E[D^q]$ is the total energy of the defect-containing Y_2O_3 (Y_2O_3:Bi^{3+}) cell with a charge q, E^0 is the total energy of the defect-free Y_2O_3 (Y_2O_3:Bi^{3+}), μ_i is the chemical potential of the element i added to (removed from) the Y_2O_3 (Y_2O_3:Bi^{3+}) cell to generate a point defect, E_v is the valence band maximum (VBM) of the defect-free Y_2O_3, ΔV is the shift in the VBM in the defective cell by a point defect, relative to that in the defect-free Y_2O_3, and ε_F is the Fermi level referenced to E_v.

Table 3 Point defect formation energies in bixbyite Y_2O_3 under extremely reducing ($\mu_Y = \mu_Y^0$) and oxidizing ($\mu_O = \mu_O^0$) conditions, the upper limits of eqn (5) and (6). V_O–Bi_{S_6} is an O vacancy in the vicinity of Bi^{3+} at the S_6 site, and the other notations are made in the same way

	Defect	Charge on defect (*e*)	Formation energy (eV) $\mu_Y = \mu_Y^0$	Formation energy (eV) $\mu_O = \mu_O^0$
Pure Y_2O_3	V_O	0	0.62	7.44
		+1	−4.05	2.77
		+2	−7.76	−0.94
	V_{S_6}	0	13.59	3.35
		−1	14.58	4.34
		−2	15.88	5.64
		−3	17.31	7.07
	V_{C_2}	0	13.71	3.47
		−1	14.80	4.56
		−2	16.21	5.97
		−3	19.34	9.10
	O_i	0	7.70	0.88
		−1	9.33	2.51
		−2	11.19	4.37
	Y_i	0	3.92	14.16
		+1	−0.70	9.54
		+2	−5.36	4.88
		+3	−8.95	1.19
	O_{C_2}	0	18.24	1.16
		−1	20.04	2.98
		−2	23.12	6.06
	Y_O	0	5.86	22.92
		+1	0.46	17.52
		+2	−4.68	12.38
		+3	−9.39	7.67
Y_2O_3:Bi	V_O–Bi_{S_6}	0	−1.16	5.55
		+1	−4.88	1.83
		+2	−8.76	−2.05
	V_O–Bi_{C_2}	0	−0.67	6.04
		+1	−4.58	2.13
		+2	−5.11	−1.60
	O_i–Bi_{S_6}	0	6.57	−0.14
		−1	8.54	1.83
		−2	11.20	4.49
	O_i–Bi_{C_2}	0	6.46	−0.25
		−1	8.31	1.60
		−2	10.89	4.18

The calculated formation energies of the point defects of yttria under extremely oxidizing ($\mu_O = \mu_O^0$) and reducing ($\mu_Y = \mu_Y^0$) conditions, when the Fermi level is at the VBM, are listed in Table 3. Between the two types of interstitial sites in the bixbyite structure, site 8a with six oxygen and six yttrium atoms at its neighbors and site 16c with six oxygen and four yttrium atoms at its neighbors, site 16c is preferred by both the yttrium and the oxygen atoms. We compared the energetic stabilities of the point defects in the pure yttria and the adjacent sites to the doped Bi atom in Y_2O_3:Bi^{3+}. Among the point defects considered in this study, only V_O and O_i prefer to be in the vicinity of the doped Bi atom at the S_6 and the C_2 sites, respectively. Other point defects have higher formation energies than those in the pure yttria.

Pure yttria at room temperature ($T = 300$ K) (Fig. 4(a)) has the same dominant defects under O-rich conditions and at atmospheric oxygen pressure ($P_{O_2} = 0.21$ atm): the V_o^{2+} defect in the p-type region and O_i, O_i^- and O_i^{2-} in the n-type region. In the O-poor limit at 300 K for pure Y_2O_3, the defects Y_i^{3+}, Y_O^{3+} and (V_o^{2+}) are competing in the p-type region, and the V_o^{2+}, V_o^+ and V_O defects become the dominant defects as it becomes n-type, following the reaction formula:

$$Y_Y^{3+} + \frac{3}{2}O_O^{2-} = Y_O^{3+} + V_Y^{3-} + \frac{3}{4}O_{2\ (g)} \qquad \text{(IV)}$$

and

$$Y_Y^{3+} + \frac{3}{2}O_O^{2-} = Y_i^{3+} + V_Y^{3-} + \frac{3}{2}V_O^{2+} + 3e + \frac{3}{4}O_{2\ (g)}. \qquad \text{(V)}$$

At heat treatment temperature and atmosphere ($T = 1300$ K, $P_{O_2} = 0.21$ atm), the dominant point defects in the pure and the

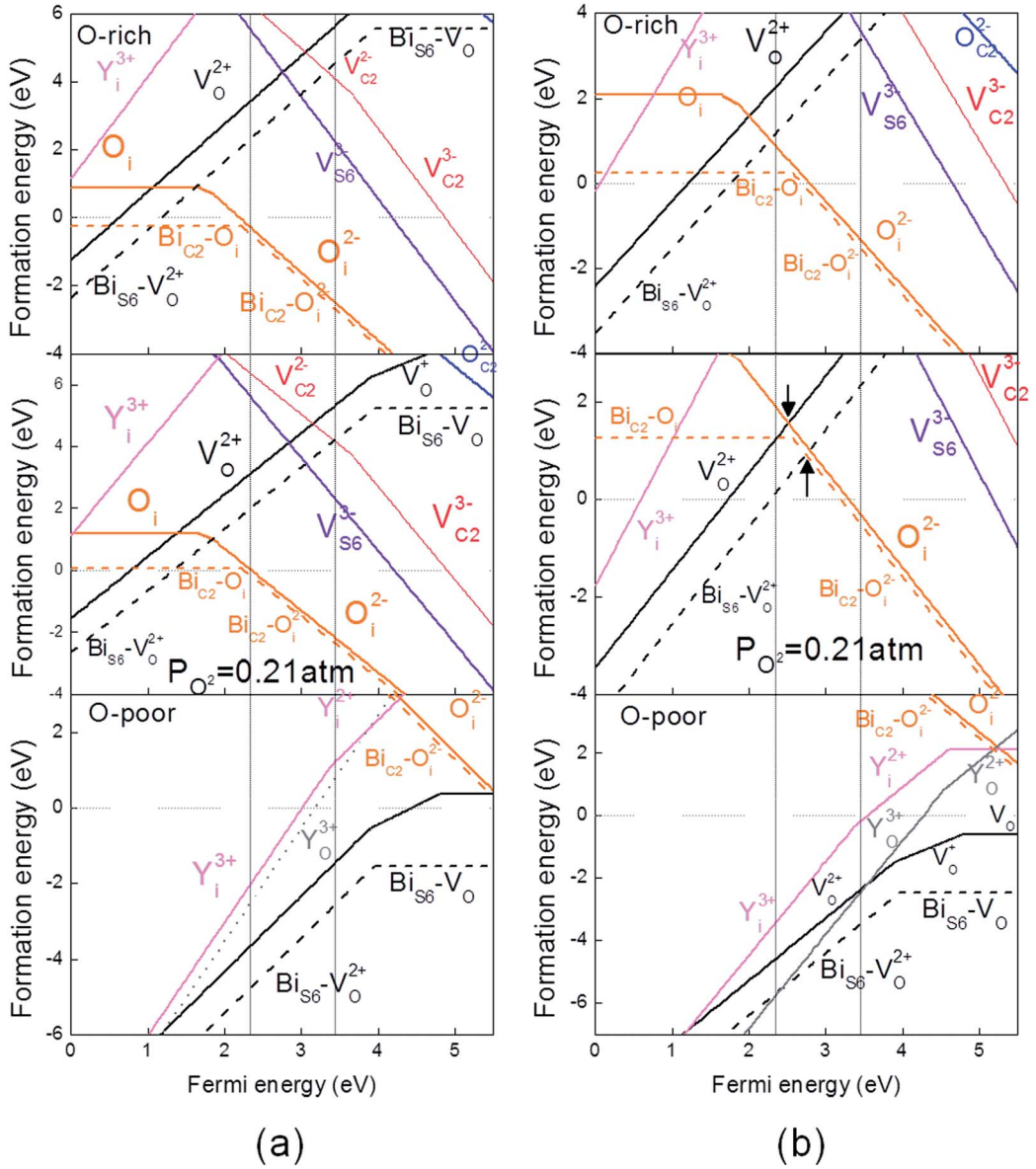

Fig. 4 Defect formation energy for $P_{O_2} = 0.21$ atm, O-rich and O-poor limits at (a) 300 K and (b) 1300 K, as a function of the Fermi level in the gap of yttria. Slopes of each line are the charges of the defects. Solid and dashed lines are the formation energies for pure and Bi^{3+}-doped Y_2O_3.

Bi-doped yttria are the oxygen Frenkel pair ((V_o^{2+}) and O_i^{2-}), as the Fermi level is pinned at the intersection of the $Bi_{S_6} - V_o^{2+}$ and the Bi_{C_2}–O_i curves. The concentrations of the defect pairs in pure and 1%-Bi doped yttria are 1.31×10^{15} cm^{-3} and 3.19×10^{16} cm^{-3}, respectively, according to the equation,

$$[V_O^{2+}] = [O_i^{2-}] = \exp\left[\frac{-\Delta E^f(q)}{k_B T}\right], \quad (8)$$

where $[V_o^{2+}]$ and $[O_i^{2-}]$ are the concentrations, and $\Delta E_f(q)$ is the defect formation energy of each defect obtained at the pinned Fermi level (Fig. 4(b)).

In the O-poor limit at $T = 1300$ K, the Bi-doped Y_2O_3 also has Y_O^{3+} due to the temperature effect. We attribute the lower formation energies of oxygen vacancies in the vicinity of the Bi^{3+} dopant to the longer Bi–O bond lengths than those of Y–O. The bond lengths of Bi–O and Y–O obtained from PBE schemes show the same tendency as those from the *ab initio* embedded cluster methods:[34] the bond lengths of Bi–O and Y–O at S_6 are larger than two of those at the C_2 site and are smaller than the last one (Table 4). The PBE method gives bond lengths and lattice constants, which are closer to the experimental values (see Table 1). As is discussed in the next section, much higher concentrations of V_o^{2+} and O_i^{2-} Frenkel defect pairs in Y_2O_3:Bi^{3+} might remarkably change the optical properties of the system during the high temperature treatment.

c. Effects of point defects on the electronic structures and optical properties of Y_2O_3 and Y_2O_3:Bi

We present the electron density of states (DOS) for the defect-containing yttria in Fig. 5. The neutral (V_O) and the singly charged oxygen vacancies (V_o^+) in the yttria induce deep donor-like levels. The doubly charged oxygen vacancy (V_o^{2+}) induces a deep unoccupied state in the middle of the yttria band gap. The O_i^{2-} defect induces occupied levels near the VBM, which are filled with oxygen 2*p* electrons. The expected photon energy absorbed by the Y_i^{3+} from the positions of the Fermi level and the induced in-gap states from the calculated DOS is 4–5 eV, which is expected to have an effect on the energy transfer or the emission from the Bi^{3+} dopant. On the other hand, Y_O^{3+} has donor-like states in the gap and also induces the level to coordinate strongly to four yttrium atoms (one S_6 and three C_2 sites). One of the expected photoexcitation energies from Y_O^{3+} is at approximately 1.2 eV, which is fatal for the NIR emitting phosphor. Note that the discussion for the defects in yttria can be applied to the same types of defects in the Y_2O_3:Bi^{3+} system when the sites are far away from the bismuth atoms.

Table 4 Calculated bond lengths between cations (Y and Bi) and oxygen in Y_2O_3 and Y_2O_3:Bi^{3+}. The notations *d*1, *d*2 and *d*3 are the cation–anion distances in sequences

Cation site	Cation element	*d*1 (Å)	*d*2 (Å)	*d*3 (Å)
S_6	Y	2.285	—	—
	Bi	2.370	—	—
C_2	Y	2.246	2.263	2.343
	Bi	2.299	2.362	2.445

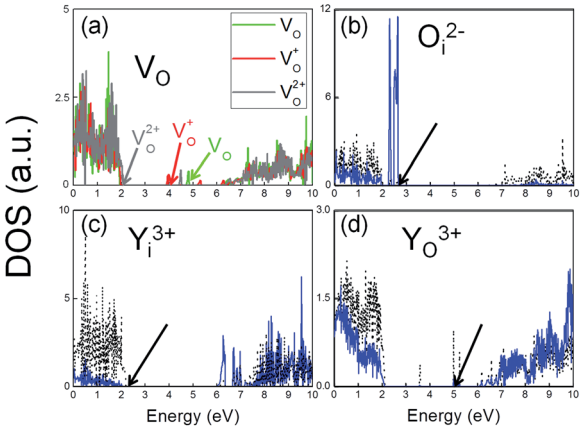

Fig. 5 Electron DOS for defect-containing Y_2O_3. The black dotted lines are the DOS of the total system containing a point defect, normalized by the number of atoms. The blue solid curves are the DOS of the defect atoms. The arrows point to the highest occupied states.

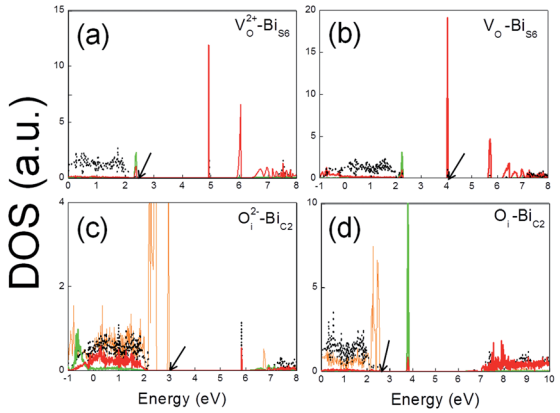

Fig. 6 Electron DOS of defective Y_2O_3:Bi^{3+}. The black dotted lines are the DOS of the total system normalized by the number of atoms; green and red solid lines are the DOS of 6*s* and 6*p* orbitals of doped Bi^{3+}; the solid orange line is DOS of the interstitial oxygen.

The energetic stability of the oxygen vacancy and the interstitial defects near the doped Bi^{3+} atom at the S_6 and the C_2 sites was demonstrated in the previous section. In Fig. 6, accordingly, the electron DOS of Bi at the S_6 and the C_2 sites that are altered by the adjacent V_o^{2+} and O_i^{2-} defects are presented. The theoretically predicted photoexcitation energy in Bi at the S_6 site by the $6s^2 \rightarrow 6s6p$ transitions is changed from 3.1 eV to 2.5 and 3.6 eV by the adjacent V_o^{2+}, as can be inferred from the positions of the two split, unoccupied 6*p* levels (Fig. 6(a)). When the oxygen vacancy is neutral, one of the 6*p* levels is occupied. The Bi atom at the C_2 site has the broad peaks of the 6*s*- and the 6*p*-orbitals below the VBM resulting from the strong hybridization with the adjacent O_i^{2-} defect atom. Hence, the photoexcitation peak from the Bi–O_i^{2-} complex is expected to have a broader peak in the higher energy region than for the defect-free case. When the adjacent oxygen interstitial is neutral, the 6*s* orbital is unoccupied, which indicates negligible photoexcitation in Bi^{3+}.

Because good phosphor should not absorb the emitted light from the dopants and waste the photon energy, we tested whether the two major defects of O_i^{2-} and V_o^{2+} absorb emitted photons from the bismuth dopants. We found that O_i^{2-} in the vicinity of Bi^{3+} at the C_2 site absorbs a photon energy of 4.08 eV (304 nm), which is much higher energy than emission from Bi^{3+}. On the other hand, V_o^{2+} in the vicinity of the S_6 site can absorb the emission from Bi^{3+} at the C_2 site such that it degrades the performance of the phosphor. Bi^{3+} at the C_2 site emits around 500 nm wavelength photons.[5–10] As shown in Fig. 6, V_o^{2+} absorbs 473 nm and 492 nm photons, which are similar in wavelength to the emitted photon from Bi^{3+}. On the other hand, O_i^{2-} does not absorb such photons (Fig. 6(c)), and thus, an oxygen interstitial will not cause harm to the PL properties of the phosphor.

The dominant point defects of Y_2O_3:Bi^{3+} annealed at high temperature have long been in question. Our DFT calculations predict that the dominant point defects are the Frenkel pair of V_o^{2+} and O_i^{2-}, with concentrations of 3.19×10^{16} cm^{-3} for 1% Bi doping, which is dense enough to significantly affect the optical properties.[35,36] From the calculated defect formation energies and the absorption wavelength of defect sites, we found that the Bi^{3+} doping increases the concentration of V_o^{2+} defects which absorb the significant amount of photons emitted not only from Bi^{3+} at the S_6 site, where V_o^{2+} is located, but also from Bi^{3+} at the C_2 site. Thus, we expect that annealing under oxygen-rich conditions is effective for achieving a high emission intensity from Bi^{3+} in the Y_2O_3 host, by preventing V_o^{2+} formation. Our prediction is well proven by the experimental results obtained with Y_2O_3:Bi^{3+} phosphors prepared under different environments in the next section.

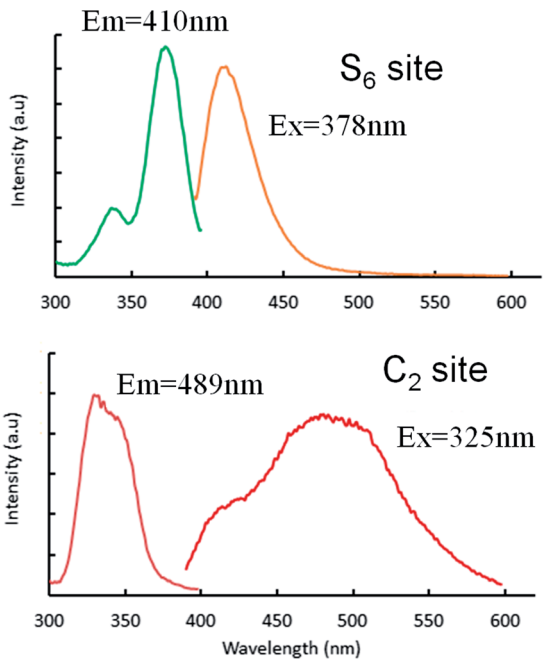

Fig. 7 PL and PLE patterns of Y_2O_3:Bi^{3+} prepared under an ambient atmosphere.

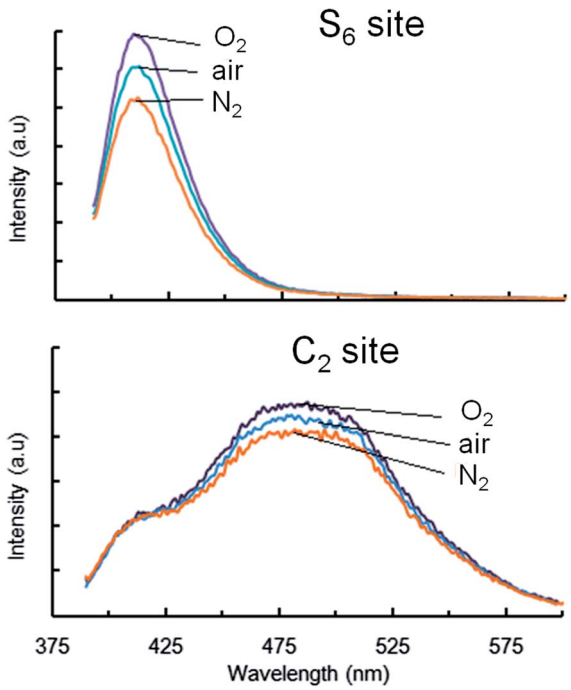

Fig. 8 PL of S_6 and C_2 sites of Y_2O_3:Bi^{3+} prepared under ambient, O_2, and N_2 atmospheres, respectively.

d. Effect of annealing atmosphere on the photoluminescence of Y_2O_3:Bi^{3+}

As mentioned earlier, several different groups applied the combustion method to obtain Y_2O_3:Bi^{3+} nanophosphors. Jacobsohn *et al.*, in particular, monitored the heat of combustion of different fuels and found that the emission properties of Bi are significantly influenced by fuels.[14] However, the heating atmosphere has not yet been monitored as a variable. Therefore we followed the combustion method reported by Jacobsohn *et al.* to make Y_2O_3:Bi^{3+} and varied the annealing atmosphere to apply our prediction to the real synthetic condition. We prepared 1% Bi-doped Y_2O_3:Bi^{3+} phosphors and annealed them at 1200 °C for 2 h under ambient conditions, oxygen-rich (O_2, >99.9%, 1 atm) and oxygen-poor atmospheres (N_2, >99.9%, 1 atm), respectively. Y_2O_3:Bi^{3+} prepared under ambient conditions showed very similar PL and PLE patterns as reported by Jacobsohn *et al.* (Fig. 7).[14] Interestingly, when the annealing atmosphere was changed to oxygen poor, both S_6 and C_2 emission decreased by ~13% at λ_{max} whereas under oxygen rich conditions, their emission increased by ~12% (Fig. 8). The increase of PL intensity can be important because the quantum efficiency of nanophosphors is often considered to be lower than 20% and hence every small increase counts for the improvement.

Conclusions

We systematically investigated the formation of point defects in the Y_2O_3:Bi^{3+} system and their effects on the optical properties. We demonstrated that the Bi-doped bixbyite yttria phosphor

has a higher defect concentration than the pure matrix. Especially at high temperature (*e.g.*, 1300 K) and at ambient pressure, the Frenkel defect pair of oxygen (V_O and O_i) is dominant in Y_2O_3:Bi^{3+}, with concentrations of 3.19×10^{16} cm^{-3} for 1% Bi doping. V_o^{2+} becomes the re-absorption center for the photons emitted from Bi^{3+} at the C_2 site, such that it degrades the efficiency of the green emission or the energy transfer from the Bi dopant to the activator atoms. Our experimental PL measurements agree well with our theoretical prediction. Therefore, we suggest high-temperature treatment under a high-oxygen partial pressure to achieve high efficiency for Y_2O_3:Bi^{3+} phosphors.

Acknowledgements

We are thankful for support from the KIST internal projects (Grant no. 2E23891) and the Converging Research Center Program through the Ministry of Science, ICT and Future Planning, Korea (Grant no. 2013K000176).

References

1 S. Ray, P. Pramanik, A. Singha and A. Roy, *J. Appl. Phys.*, 2005, **97**, 094312.
2 V. K. Rai, A. Pandey and R. Dey, *J. Appl. Phys.*, 2013, **113**, 083104.
3 X.-L. Liu, P.-X. Zhu, Y.-F. Gao and R.-H. Jin, *J. Mater. Chem. C*, 2013, **1**, 477.
4 R. H. Krishna, B. M. Nagabhushana, H. Nagabhushana, N. S. Murthy, S. C. Sharma, C. Shivakumara and R. P. S. Chakradhar, *J. Phys. Chem. C*, 2013, **117**, 1915.
5 W. Zhu, Y. Wu, A. Leto, J. Du and G. Pezzotti, *J. Phys. Chem. A*, 2013, **117**, 3599.
6 P. Chung, H. Chung and P. H. Holloway, *J. Vac. Sci. Technol., A*, 2007, **25**, 61.
7 L. S. Chi, R. S. Liu and B. J. Lee, *J. Electrochem. Soc.*, 2005, **152**, J93.
8 G. Ju, Y. Hu, C. Li, X. Wang, Z. Mu, H. We and F. Kang, *J. Lumin.*, 2012, **132**, 1853.
9 X.-T. Wei, J.-B. Zhao, Y.-H. Chen, M. Yin and Y. Li, *Chin. Phys. B*, 2010, **19**, 077804.
10 X. Y. Huang, X. H. Ji and Q. Y. Zhang, *J. Am. Ceram. Soc.*, 2011, **94**, 833.
11 J.-L. Yuan, X.-Y. Zeng, J.-T. Zhao, Z.-J. Zhang, H.-H. Chen and X.-X. Yang, *J. Phys. D: Appl. Phys.*, 2008, **41**, 105406.
12 J. J. Kingsley and K. C. Patil, *Mater. Lett.*, 1988, **6**, 427.
13 D. Zhao, S. Seo, H. Zhang, B. S. Bae and W. Qin, *J. Nanosci. Nanotechnol.*, 2010, **10**, 2036.
14 L. G. Jacobsohn, M. W. Blair, S. C. Tomga, L. O. Brown, B. L. Bennett and R. E. Muenchausen, *J. Appl. Phys.*, 2008, **104**, 124303.
15 A. Alkauskas, J. L. Lyons, D. Steiauf and C. G. Van de Walle, *Phys. Rev. Lett.*, 2012, **109**, 267401.
16 Q. Yan, A. Janotti, M. Scheffler and C. G. Van de Walle, *Appl. Phys. Lett.*, 2012, **100**, 142110.
17 A. Janotti and C. G. Van de Walle, *Rep. Prog. Phys.*, 2009, **72**, 126501.
18 J. L. Lyons, A. Janotti and C. G. Van de Walle, *Phys. Rev. Lett.*, 2012, **108**, 156403.
19 C. G. Van de Walle and A. Janotti, *Phys. Status Solidi B*, 2011, **248**, 19.
20 W. Kohn and L. J. Sham, *Phys. Rev.*, 1965, **140**, A1133.
21 G. Kresse and J. Hafner, *Phys. Rev. B: Condens. Matter Mater. Phys.*, 1993, **47**, 558.
22 H. J. Monkhorst and J. D. Pack, *Phys. Rev. B: Condens. Matter Mater. Phys.*, 1976, **13**, 5188.
23 J. Zheng, G. Ceder, T. Maxisch, W. K. Chim and W. K. Choi, *Phys. Rev. B: Condens. Matter Mater. Phys.*, 2006, **73**, 104101.
24 J. P. Perdew, J. A. Chevary, S. H. Vosko, K. A. Jackson, M. R. Pederson, D. J. Singh and C. Fiolhais, *Phys. Rev. B: Condens. Matter Mater. Phys.*, 1992, **46**, 6671–6687.
25 J. P. Perdew, K. Burke and M. Ernzerhof, *Phys. Rev. Lett.*, 1996, **77**, 3865.
26 J. P. Perdew, K. Burke and M. Ernzerhof, *Phys. Rev. Lett.*, 1997, **78**, 1396.
27 S. L. Dudarev, G. A. Botton, S. Y. Savrasov, C. J. Humphreys and A. P. Sutton, *Phys. Rev. B: Condens. Matter Mater. Phys.*, 1988, **57**, 1505.
28 F. Furche, *Phys. Rev. B: Condens. Matter Mater. Phys.*, 2001, **64**, 195120.
29 A. S. Kaygorodov, V. V. Ivanov, V. R. Khrustov, Yu. A. Kotov, A. I. Medvedev, V. V. Osipov, M. G. Ivanov, A. N. Orlov and A. M. Murzakaev, *J. Eur. Cera. Soc.*, 2007, **27**, 1165.
30 D. R. Stull and H. Prophet, *JANAF Thermochemical Tables, Natl. Bur. Stan. (U.S.)*, DC: U.S. GPO, Washington, 2nd edn, 1971.
31 K. K. Kelley, *Contributions to Data on Theoretical Me Tallurgy: Y, Heats of' Fusion of Inorganic Substances*, U.S. Bur. Mines Bull., 1936, vol. 393, pp. 166.
32 C. R. Stanek, K. J. McClellan, M. R. Levy and R. W. Grimes, *IEEE Trans. Nucl. Sci.*, 2008, **55**, 1492.
33 A. Baldereschi, S. Baroni and R. Resta, *Phys. Rev. Lett.*, 1988, **61**, 734.
34 F. Réal, V. Vallet, J. P. Flament and J. Schamps, *J. Chem. Phys.*, 2007, **127**, 104705.
35 M. Peressi, N. Binggeli and A. Balderreschi, *J. Phys. D: Appl. Phys.*, 1988, **31**, 1273.
36 L. Schmidt-Mende and J. L. Macmanus-Driscoll, *Mater. Today*, 2007, **10**, 40.

